Asian Journal of Chemistry; Vol. 37, No. 7 (2025), 1796-1802

ASIAN JOURNAL OF CHEMISTRY

https://doi.org/10.14233/ajchem.2025.33982

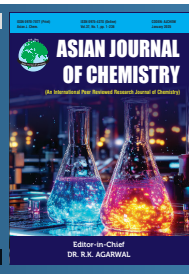

Green Synthesis of Platinum@Silver (Pt@Ag) Bimetallic Nanoparticles Using *Carica papaya* Aqueous Leaf Extract for Catalytic Reduction of Dyes and their Antimicrobial Activity

T. JAYAMANI[1,2], T. AUGUSTINE ARUL PRASAD[1,*] and B. SCHOLASTICA MARY VITHIYA[3]

[1]PG and Research Department of Chemistry, Dwarakadoss Goverdhandoss Vaishnav College (Autonomous), (Affiliated to University of Madras) Chennai-600106, India
[2]Department of Chemistry, Alpha College of Engineering, Thirumazhisai, Chennai-600124, India
[3]PG and Research Department of Chemistry, Auxilium College (Autonomous), (Affiliated to Thiruvalluvar University, Vellore), Vellore-632006, India

*Corresponding author: E-mail: augustineap@gmail.com

Received: 3 May 2025; *Accepted*: 27 June 2025; *Published online*: 30 June 2025; AJC-22056

This study presents a green, plant-mediated synthesis of platinum@silver (Pt@Ag) bimetallic nanoparticles using aqueous extracts of *Carica papaya* leaves as a bio-reducing and capping agent. The synthesized nanoparticles were characterized *via* UV-Vis spectroscopy, FTIR, XRD, SEM and HRTEM, confirming their crystalline nature, face-centered cubic structure and nanoscale core-shell morphology. FTIR analysis revealed functional groups such as hydroxyl and amide, supporting the biomolecular involvement in nanoparticle stabilization. The Pt@Ag nanoparticles exhibited a significant catalytic activity in the reduction of methylene blue and Congo red dyes, with a pseudo-first-order rate constant of 0.00512 min^{-1} for methylene blue. Furthermore, the antimicrobial studies demonstrated significant inhibition zones against both Gram-positive and Gram-negative bacteria, outperforming standard antibiotics in some cases. The observed synergistic effects of platinum and silver enhance both redox and ion-release mechanisms, making these nanoparticles promising candidates for environmental remediation and biomedical applications.

Keywords: Platinum@Silver nanoparticles, *Carica papaya*, Antimicrobial activity, Degradation activity, Organic dyes.

INTRODUCTION

Metal nanoparticles, including platinum, platinum, gold, and silver, have garnered significant attention due to their exceptional physico-chemical properties, which encompass catalytic activity, electrical conductivity, thermal properties, surface plasmon resonance, and biological activities [1]. These unique characteristics arise from their large surface area-to-volume ratio and quantum size effects, making them suitable for diverse applications such as catalysis, electronics, optics and biomedicine [2,3]. Among these, bimetallic nanoparticles, which combine two different metals, offer the potential for enhanced properties and functionalities compared to their monometallic counterparts [4]. The synergistic effects in bimetallic nanoparticles, arising from their nanoalloy or core-shell structures, lead to superior catalytic activity and efficiency, making them attractive for fine-chemicals synthesis and transformations [5]. Research into the development of eco-friendly technologies should focus on the synthesis and design of clearly defined metallic and bimetallic nanoparticles as well as an evaluation of the size-and shape-dependent features that impact their potential uses [6].

The synthesis of nanoparticles can be achieved through various chemical and physical methods. However, these traditional methods often involve the use of hazardous chemicals, high energy consumption, and the generation of toxic byproducts, raising environmental concerns. As a result, there is growing interest in green synthesis approaches that utilize biocompatible and eco-friendly materials. Green synthesis harnesses the reducing and capping capabilities of non-toxic plant-based secondary metabolites, offering an eco-conscious alternative [7]. The utilization of plant extracts, microorganisms or other biological sources for nanoparticle synthesis has emerged as a sustainable approach, aligning with the principles of green chemistry. Plant-mediated synthesis, in particular, has gained prominence due to

its cost-effectiveness, ease of implementation, availability of diverse biomolecules and ability to facilitate rapid nanoparticle synthesis [8]. Plant extracts contain a mixture of various organic compounds such as alkaloids, flavonoids and terpenoids, act as both reducing and stabilizing agents, enabling the formation of stable nanoparticles without the need for additional toxic chemicals [9]. The exploration of plant extracts for nanoparticle synthesis provides a unique avenue for producing nanomaterials with tailored properties and enhanced biocompatibility, paving the way for various applications in catalysis, biomedicine, and environmental remediation [10-12]. By employing green synthesis methods, the negative environmental impacts associated with conventional nanoparticle production can be minimized, leading to a more sustainable and responsible approach to nanotechnology [13].

In this context, *Carica papaya*, commonly known as papaya, presents a promising candidate for green synthesis due to its rich source of bioactive compounds. Belonging to the Caricaceae family, *C. papaya* possesses a diverse array of secondary metabolites, including alkaloids, flavonoids, amino acids, lipids and carbohydrates, which are known for their reducing and stabilizing properties [14]. These biomolecules can facilitate the reduction of metal ions into their corresponding nanoparticles and provide a capping effect, preventing agglomeration and ensuring stability. Papaya (*C. papaya*) extract has been successfully utilized in the green synthesis of various metal nanoparticles, including silver, gold and copper oxide, demonstrating its effectiveness and versatility as a biological reducing agent. In addition to its role in nanoparticle synthesis, *C. papaya* exhibits a range of biological activities such as antioxidant, antimicrobial and anticancer properties, which may be further enhanced when incorporated into nanoparticle formulations [15-19]. The use of *C. papaya* extract offers a dual advantage by providing both a sustainable synthesis route and endowing the resulting nanoparticles with enhanced bioactivity [14].

Considering the aforementioned advantages, this study focuses on the green synthesis of platinum@silver (Pt@Ag) bimetallic nanoparticles using the aqueous extract of *C. papaya* and the evaluation of their catalytic and antimicrobial properties. The selection of platinum and silver as the constituent metals is based on their established catalytic activity and antimicrobial efficacy, respectively. Platinum nanoparticles are known for their exceptional catalytic properties in various chemical reactions, including reduction of dyes, oxidation of alcohols and hydrogenation of alkenes [20]. Silver nanoparticles, on the other hand, exhibit broad-spectrum antimicrobial activity against bacteria, fungi, and viruses, making them attractive for biomedical applications [21,22]. By combining platinum and silver into a bimetallic nanostructure, synergistic effects can be achieved, leading to enhanced catalytic activity and antimicrobial efficacy compared to their monometallic counterparts.

The novelty of this research lies in the combination of silver and platinum into a bimetallic nanostructure using a green synthesis approach, leveraging the reducing and capping capabilities of the aqueous extract of *C. papaya* leaves [23]. Furthermore, the evaluation of the catalytic and antimicrobial properties of the synthesized bimetallic nanoparticles aims to provide insights into their potential applications in environmental remediation and biomedicine.

EXPERIMENTAL

Hexachloro platinic acid hexahydrate [$H_2PtCl_6{\cdot}6H_2O$] as the source of platinum ions and silver nitrate ($AgNO_3$) as the source of silver ions were procured from Alfa Aesar and used without further purification. Sodium borohydride ($NaBH_4$), methylene blue and Congo red dyes were procured from Merck Ltd., India. All the solutions were prepared in demineralized water.

Preparation of leaf extract of *Carica papaya*: Fresh *C. papaya* leaves were collected from the local market of Chennai city, India and washed with demineralized water and air dried for two weeks. It was then freshly powdered and stored. The leaf powder (0.1 g) was added in 125 mL of demineralized water and heated at 85 ºC and filtered using whatmann filter paper. The filtrate was kept at 5 ºC as reducing and stabilizing agent for further study.

Green synthesis of bimetallic Pt@Ag core shell NPs: To a 10 mL of 0.5 mM of $H_2PtCl_6{\cdot}6H_2O$ aqueous solution, 10 mL of *C. papaya* leaves extract was added slowly for 10 min with stirring at 1500 rpm for 1 h at 80 ºC. The reduction process Pt^{4+} to Pt^0 nanoparticle is followed by the colour of the solution changes from yellow to greyish brown indicating the formation of PtNPs. To this PtNPs, 10 mL of 0.5 mM of aqueous $AgNO_3$ solution added slowly for 10 min with stirring at 1500 rpm for 1.5 h at 80 ºC. The green synthesized Pt@Ag core shell NPs were separated by centrifuging at 3500 rpm for 20 min and dried in an oven at 60 ºC for 2 h. The purified bimetallic Pt@Ag core shell NPs were subjected to the characterization studies.

Antimicrobial study: The antimicrobial activity of synthesized Pt@Ag core shell NPs was evaluated using well diffusion method [24,25]. The bacterial strains *Escherichia coli* (MTCC 443), *Bacillus subtilis* (MTCC441), *Salmonella typhi* (MTCC 98), *Staphylococcus aureus* (MTCC96) and fungal strains *Candida albicans* (MTCC 227), *Aspergillus niger* (MTCC404), *Aspergillus flavus* (MTCC277), and *Penicillium chrysogenum* (MTCC5108) were obtained from MTCC, IMTECH, Chandigarh, India.

Procedure for reduction of dyes: The reduction of methylene blue and Congo red dyes using $NaBH_4$ in the presence of Pt@Ag NPs nanoparticle was carried out to demonstrate the catalytic activity of the prepared bimetallic nanoparticles. A solution of sodium borohydride (1 mL of 10 mM) was mixed ether with methylene blue dye or Congo red dye (1.5 mL of 1 mM) and the mixture was made upto 10 mL using doubled distilled water and then stirred for 5 min. To these two solutions, sufficient quantities of green synthesized Pt@Ag NPs nanoparticles were added separately and the UV-Vis spectra were recorded at regular intervals of time.

Characterization: The formation of Pt@Ag bimetallic nanoparticles was confirmed by visual colour changes and characterized by UV-Visible spectrophotometer (JASCO, V-650) instrument. FTIR (JASCO, FTIR-4100) was used to determine the functional group of green synthesized Pt@Ag core shell NPs, which was compared to aqueous extract of *C. papaya* leaf. D8 Advance (Bruker) D8 Goniometer instrument was used

to analyze the crystallinity of bimetallic nanoparticles. The SEM observations were performed on Carl Zeiss MA15/EVO 18 scanning electron microscope. High resolution transmission electron microscope (HRTEM, JEM 3010, JEOL,300 kV) was used to analyze the shape, size and structure of Pt@ AgNPs sample at 200 kV and the filament is LaB6.

RESULTS AND DISCUSSION

UV-Vis spectra: The UV-Visible absorption spectrum of Pt@Ag nanoparticles exhibited a strong and sharp peak at 314 nm, indicative of the surface plasmon resonance (SPR) behaviour of metallic nanoparticles shown in (Fig. 1). This absorption peak lies within the expected range for silver and platinum nanostructures, although pure silver nanoparticles typically exhibit SPR around 400-450 nm. The blue-shift to 314 nm suggests either nanoscale particle size increase, alloy formation or core-shell Pt@Ag interactions. The high absorbance intensity (~4 a.u.) also implies a high concentration of nanoparticles with uniform size distribution. The sharpness of the peak confirms good monodispersity and crystalline surface structure. This is in alignment with the XRD data, which confirmed a face-centered cubic (FCC) structure and nanocrystalline nature. Previous studies have reported similar blue-shifted SPR peaks in Pt-Ag hybrid nanostructures, which are attributed to the electronic interactions between Pt and Ag atoms. These shifts correlate with enhanced catalytic properties, making these nanoparticles suitable for photocatalytic dye degradation and biological applications.

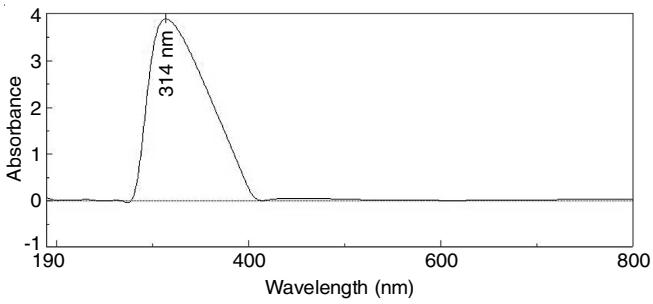

Fig. 1. UV-Vis spectrum of platinum@silver nanoparticles

FTIR spectra: The FTIR spectrum of the *C. papaya* leaf extract exhibited several key peaks indicative of phytochemical constituents involved in nanoparticle synthesis (Fig. 2a), which exhibited the broad O-H stretching around 3426.89 cm^{-1}, C-H stretching at 2922.59 and 2855.1 cm^{-1} and C=O stretching at 1722.00 cm^{-1}. These groups are typical of polyphenols, flavonoids and other reducing agents. The FTIR spectrum of Pt@Ag

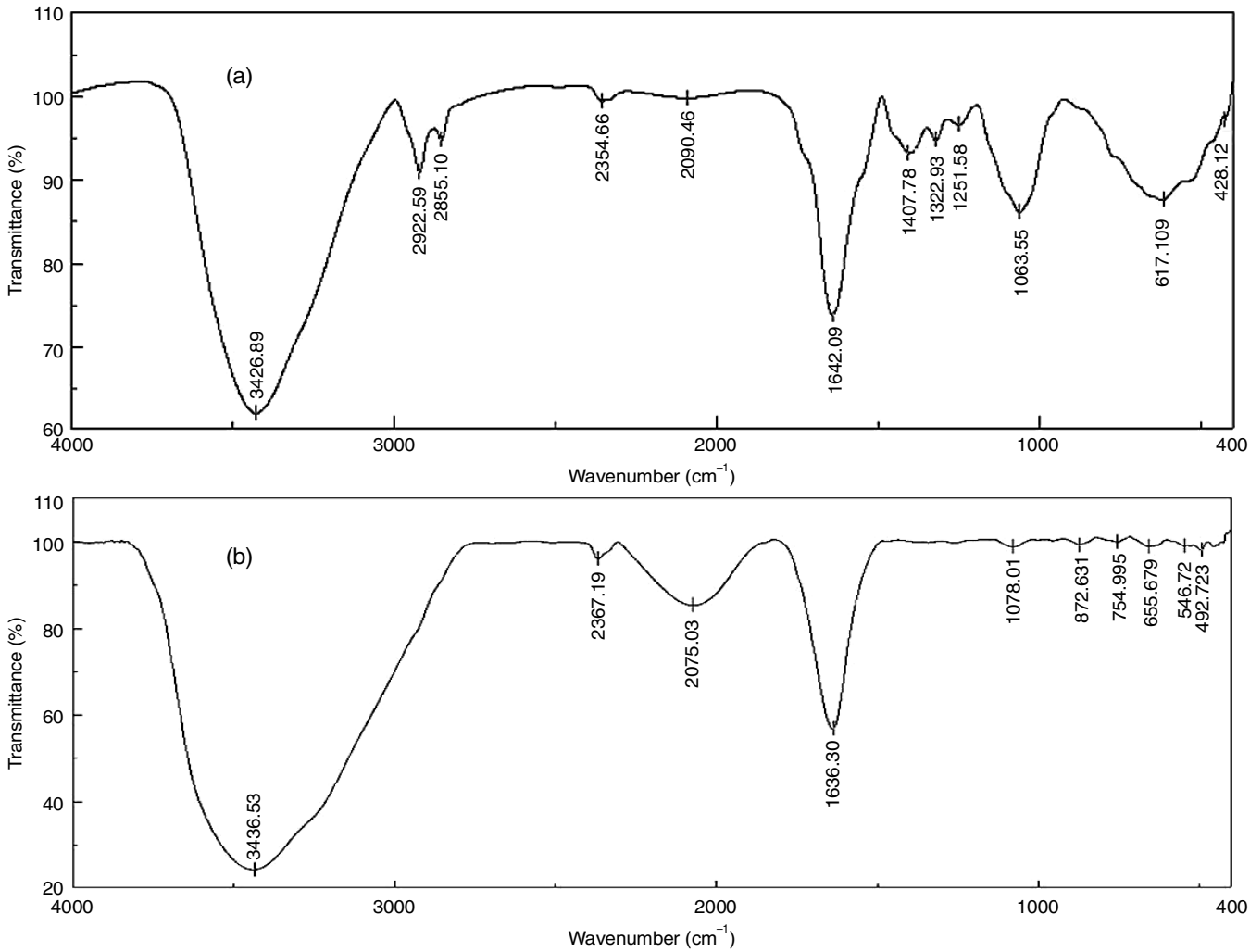

Fig. 2. FTIR analysis of (a) *Carica papaya* leaf extract and (b) platinum@silver nanoparticles

nanoparticles (Fig. 2b) showed the shifted and diminished peaks corresponding to the original functional groups in the leaf extract, suggesting their role in metal ion reduction and nanoparticle stabilization. Notable peaks include O-H stretching at 3436.53 cm^{-1}, C-H stretching at 2921.9 cm^{-1} and C=O stretching at 1633.9 cm^{-1}, alongside the appearance of new peaks in the fingerprint region indicative of metal-oxygen bonds. The low wavenumber peaks (below 600 cm^{-1}) suggest metal-oxygen or metal-metal bond formation, typical of Pt-Ag nanoparticle systems. The broad OH and carbonyl/amine features support the use of biomolecules for nanoparticle synthesis and stabilization, which is common in green synthesis of Pt@Ag NPs. The presence of C-N, O-H and amide bands (1400-1000 cm^{-1}) supports the biogenic origin. These functional groups may stem from proteins, enzymes or polysaccharides-indicative of microbial involvement in synthesis or capping [24-26].

XRD studies: The diffraction patterns obtained at various 2θ angles exhibit significant peaks, which is the characteristic of the face-centered cubic (fcc) crystal structure and a distinctive feature of both silver (Ag) and platinum (Pt) (Fig. 3). These peaks were observed at approximately 38º, 44º, 64º and 77º, corresponding to the (111), (200), (220) and (311) planes of the fcc structure, respectively. This matches well with the standard JCPDS patterns for silver (JCPDS No. 04-0783) and platinum (JCPDS No. 04-0802) [27].

The key observation from the XRD data is the overlap of the diffraction peaks for Ag and Pt (Table-1). This suggests that the nanoparticles are likely composed of either a Pt@Ag core-shell structure or a Pt-Ag alloy. The core-shell structure

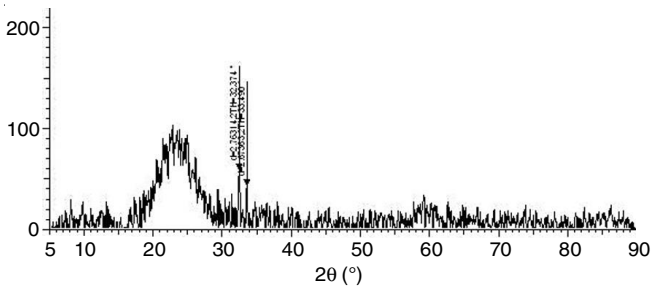

Fig. 3. XRD image of platinum@silver nanoparticles after green synthesis

would involve a core of platinum (Pt) surrounded by a shell of silver (Ag), whereas an alloy structure would result from the uniform mixing of Pt and Ag at the atomic level. Both scenarios are plausible based on the XRD peaks observed [28-30]. The broadening of the diffraction peaks is indicative of the nanoparticles being in the nanometer size range, typically less than 20 nm. This is supported by the size calculation from the Debye-Scherrer's equation, which gives an approximate crystallite size. The broad peaks in XRD are a hallmark of nanocrystalline materials due to the increased number of grain boundaries, which cause a decrease in the coherence length of the crystalline domains. The absence of additional peaks corresponding to oxide or impurity phases further suggests that the nanoparticles are of high purity, with no significant secondary phases detected [31,32].

Morphological studies: The SEM images (Fig. 4) reveal a dense arrangement of bimetallic nanoparticles, indicating the potential aggregation of particles, which is a common pheno-

TABLE-1
XRD PEAK INTERPRETATION OF PLATINUM@SILVER BIMETALLIC NANOPARTICLES

Feature	Observation	Interpretation
Peak positions (2θ)	~38º, 44º, 64º, 77º	Match fcc structure of Ag and Pt
Peak assignment	(111), (200), (220), (311)	Typical of metallic nanocrystals
Peak broadness	Broad peaks	Indicates nanocrystalline nature (< 20 nm)
Phase purity	No additional peaks	High purity Pt@Ag nanoparticles

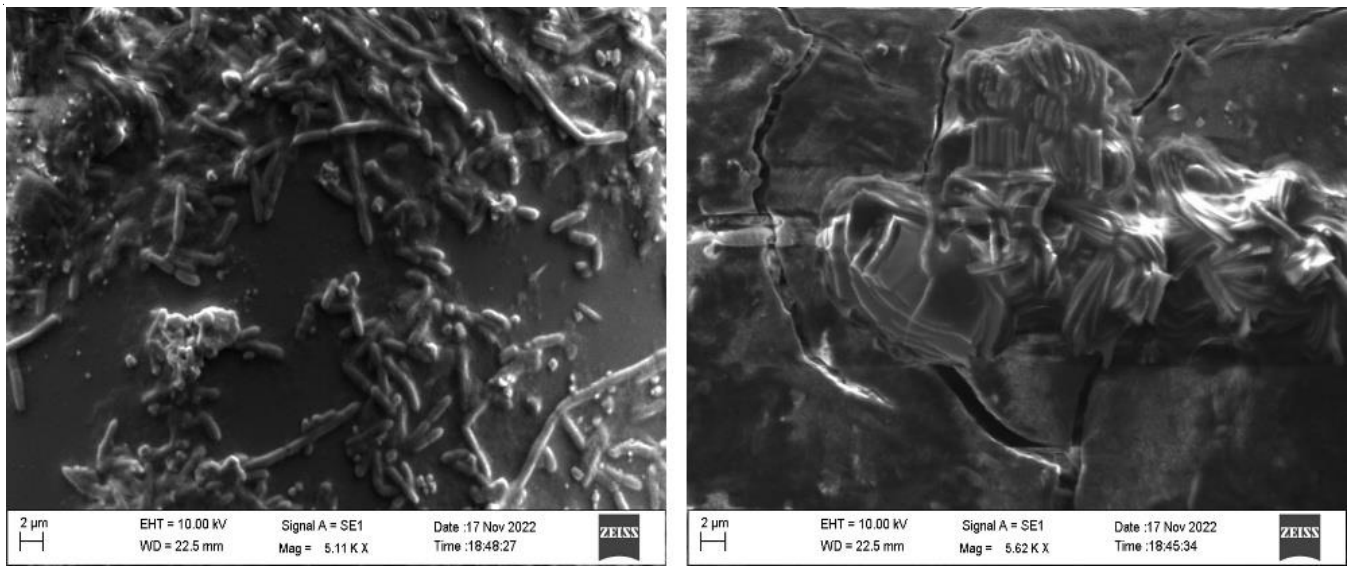

Fig. 4. SEM imaging of platinum@silver nanoparticles after green synthesis

menon in the nanoparticle synthesis. This aggregation could be due to van der Waals forces, which may cause some degree of nanoparticle clumping. The average particle size, observed to be in the nanometer range, further supports the synthesis of Pt@Ag nanoparticles. These shapes can influence the surface reactivity, as nanoparticles with higher surface area-to-volume ratios often exhibit increased reactivity. This suggests that the Pt@Ag nanoparticles are likely to be effective in applications such as catalysis and drug delivery [28,29].

The HRTEM images (Fig. 5) provide further details on the size distribution and crystalline nature of the Pt@Ag nanoparticles. The first image (Fig. 5a), with a scale bar of 5 nm, shows well-defined nanoparticles exhibiting lattice fringes characteristic of crystalline structures, which are typically seen in face-centered cubic (fcc) metals such as Pt and Ag. This confirms the crystalline nature of the bimetallic nanoparticles and supports the findings from the XRD analysis that indicated an fcc structure for both platinum and silver. The lattice spacing visible in the TEM image correlates with the interplanar distances of the (111) plane of both Ag and Pt, as previously identified by XRD.

In the second TEM image (scale bar of 20 nm, Fig. 5b), a mixture of spherical and oval-shaped nanoparticles is observed, with some nanoparticles showing a core-shell structure, particularly Pd at the core and Ag at the shell. This observation aligns with the XRD data, which suggested that the Pt@Ag nanoparticles could be either core-shell structures or Pt-Ag alloy nanoparticles. The contrast variation in the image indicates different electron densities between the Pd core and the Ag shell, further supporting the formation of a core-shell structure [28,29].

Antimicrobial activity: The green synthesized Pt@Ag bimetallic nanoparticles were tested against four bacterial strains *viz*. *Bacillus cereus*, *Escherichia coli*, *Staphylococcus aureus* and *Salmonella typhi*. The zone of inhibition (ZOI) increased with the nanoparticle concentrations (Table-2). Remarkably, the Pt@Ag bimetallic nanoparticles demonstrated the greater inhibition zones than the standard antibiotic azithromycin particularly against Gram-negative bacteria such as *E. coli* and *S. typhi*. The strong antimicrobial effect of Pt@Ag bimetallic nanoparticles is attributed to the synergistic action of platinum and silver, which can disrupt microbial membranes through redox activity and reactive oxygen species generation. Their small size and surface chemistry, characterized by functional groups like O-H and amide bonds, enhance the cellular interaction and penetration. These results corroborate with the

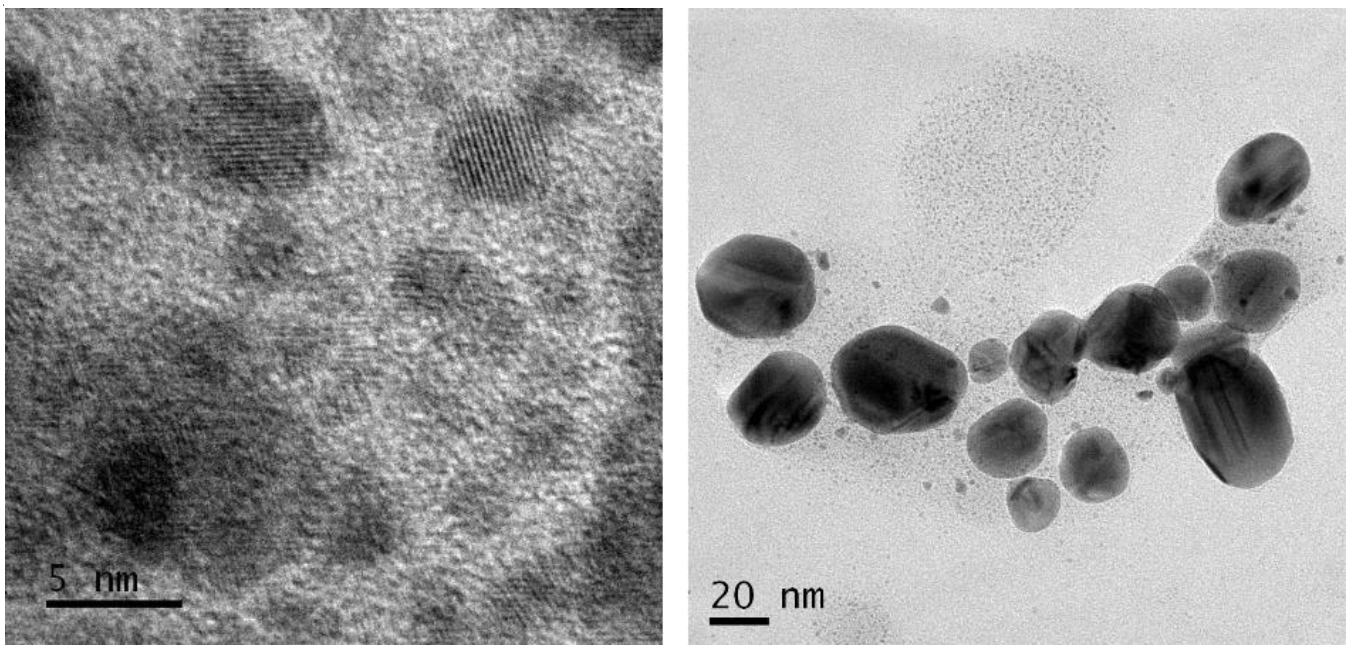

Fig. 5. HRTEM images of green synthesized platinum@silver bimetallic nanoparticles

TABLE-2
INHIBITORY CONCENTRATION OF Pt@Ag BIMETALLIC NANOPARTICLES WITH SELECTED BACTERIA AND FUNGAL SPECIES

Name of the test strains	Zone of inhibition (mm)				
	0 µL/well	25 µL/well	50 µL/well	75 µL/well	100 µL/well
Bacillus cereus	–	12	13	13	13
Escherichia coli	–	23	24	25	26
Staphylococcus aureus	–	24	25	26	28
Salmonella typhi	–	27	28	30	32
Aspergillus flavus	–	11	12	14	16
Aspergillus niger	–	10	12	14	15
Candida albicans	–	13	14	15	16
Penicillium chrysogenum	–	8	10	12	14

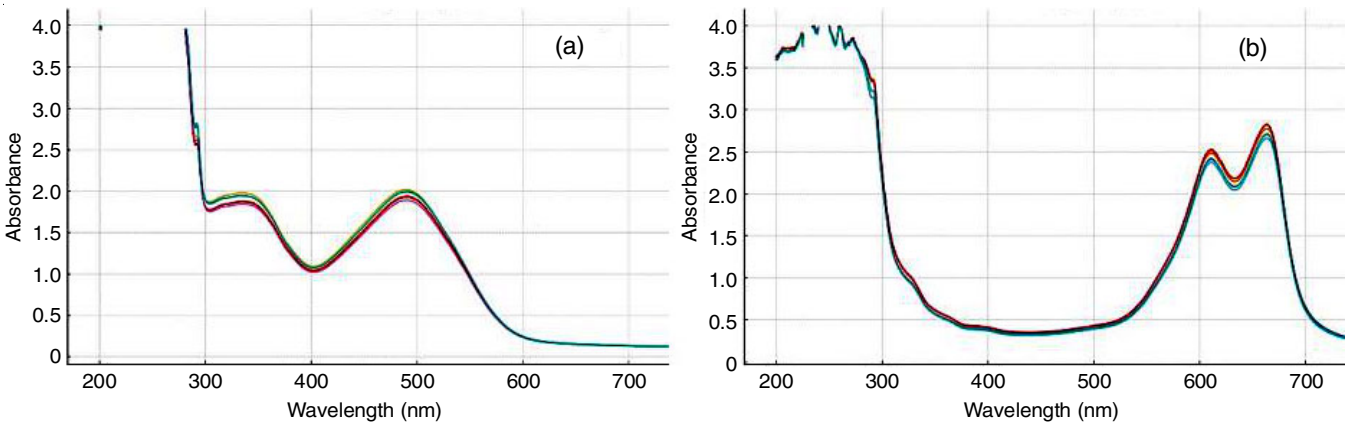

Fig. 6. Absorbance spectra of (a) Congo red and (b) methylene blue with platinum@silver bimetallic nanoparticles from 0 to 10 min

prior studies highlighting Pd-Ag systems' dual redox and ion-releasing mechanisms in the antimicrobial applications [33,34].

The antifungal efficacy exhibited by the synthesized Pt@Ag bimetallic nanoparticles against selected fungal strains suggests a promising potential for their application in antimicrobial formulations. The well diffusion method revealed distinct zones of inhibition, confirming the broad-spectrum antifungal activity of the bimetallic nanoparticles. These findings agree with prior reports where bimetallic nanoparticles demonstrated enhanced antimicrobial activity due to synergistic effects between the constituent metals [35]. The enhanced bioactivity of Pt@Ag bimetallic nanoparticles can be attributed to their unique surface chemistry and core-shell structure, which allows efficient interaction with fungal cell membranes. Silver is known to release Ag^+ ions that disrupt cell wall synthesis, damage membrane integrity and interfere with vital enzymatic functions, leading to cell death. The presence of platinum likely stabilizes the silver nanoparticles and further enhances ROS generation, contributing to oxidative stress within the fungal cells.

The results obtained are consistent with standard methods for evaluating antifungal agents and the agar-well diffusion technique employed in this study proved effective in screening nanoparticle-based antifungal compounds. However, while *in vitro* results are promising, further studies are essential to understand the precise mechanisms of action, assess cytotoxicity towards human cells, and evaluate the stability and bioavailability of Pt@Ag NPs in the biological systems.

Dye reduction activity and pseudo-first-order kinetic studies: The absorption spectra of Congo red dye treated with Pt@Ag bimetallic nanoparticles show a consistent decrease in absorbance over time, demonstrating the catalytic degradation (Fig. 6a). This behaviour indicates efficient electron transfer facilitated by the bimetallic nanoparticles, which break the azo bond within the dye molecules. The UV-spectrum of methylene blue dye also revealed the decreasing absorbance values (Fig. 6b), particularly around the λ_{max} of 664 nm. The green synthesized Pt@Ag bimetallic nanoparticles effectively degraded the dye, as evidenced by a steady decrease in intensity with increasing time [36].

A pseudo-first-order kinetic model was applied using ln (A/A_o) *versus* time. Although the degradation followed a trend, at ~201 nm showed a low linearity ($R^2 = 0.0009$) and a small rate constant ($k = 2.94 \times 10^{-5}$ min^{-1}) suggesting a limited kinetic uniformity at this wavelength. Nonetheless, the degradation activity was observable and attributed to the redox-active surface of Pt@Ag bimetallic nanoparticles. In case of methylene blue, the pseudo-first-order kinetics at 664 nm yielded a rate constant of 0.00512 min^{-1} with a correlation coefficient of $R^2 = 0.650$. This supports a reliable kinetic model and confirms that Pt@Ag bimetallic nanoparticles promote efficient catalytic reduction.

Conclusion

The study successfully demonstrates the synthesis, structural integrity and degradation potential of biosynthesized Pt@Ag bimetallic nanoparticles from the aqueous extract of *Carica papaya* leaf through the physico-chemical and functional approach. FTIR analysis confirmed the presence of biologically relevant functional groups such as O-H, C=O and C-N, supporting the microbial involvement in the synthesis. SEM and TEM analyses revealed nanoparticle morphologies ranging from 5-30 nm, including clear evidence of lattice fringes and core-shell or alloy structures indicative of bimetallic crystallinity. XRD results further validated the formation of pure, nanocrystalline face-centered cubic (fcc) Pt@Ag phases with no detectable impurities. The Pt@Ag nanoparticles exhibited strong catalytic activity toward the reduction of methylene blue dye, which showed the significant absorbance decay at 664 nm with a pseudo-first-order rate constant of 0.00512 min^{-1}, demonstrating the efficient redox activity. While Congo red dye showed the less pronounced kinetics. These findings confirm the multifunctionality of biosynthesized Pt@Ag bimetallic nanoparticles, combining the structural precision with practical catalytic performance, making them promising candidates for environmental remediation applications, particularly in the degradation of hazardous azo and cationic dyes.

CONFLICT OF INTEREST

The authors declare that there is no conflict of interests regarding the publication of this article.

REFERENCES

1. R. Kaur, P. Avti, V. Kumar and R. Kumar, *Nano Express*, **2**, 20005 (2021); https://doi.org/10.1088/2632-959X/abf42a

2. B.W. Boote, H. Byun and J. Kim, *J. Nanosci. Nanotechnol.*, **14**, 1563 (2014); https://doi.org/10.1166/jnn.2014.9077
3. K.S. Siddiqi and A. Husen, *Nanoscale Res. Lett.*, **11**, 482 (2016); https://doi.org/10.1186/s11671-016-1695-z
4. H. Jung, M.E. King and M.L. Personick, *Curr. Opin. Colloid Interface Sci.*, **40**, 104 (2019); https://doi.org/10.1016/j.cocis.2019.02.004
5. I. Notar Francesco, F. Fontaine-Vive and S. Antoniotti, *ChemCatChem*, **6**, 2784 (2014); https://doi.org/10.1002/cctc.201402252
6. P.K. Dikshit, J. Kumar, A.K. Das, S. Sadhu, S. Sharma, S. Singh, P.K. Gupta and B.S. Kim, *Catalysts*, **11**, 902 (2021); https://doi.org/10.3390/catal11080902
7. G. Marslin, K. Siram, Q. Maqbool, R.K. Selvakesavan, D. Kruszka, P. Kachlicki and G. Franklin, *Materials*, **11**, 940 (2018); https://doi.org/10.3390/ma11060940
8. J. Sandhya and S. Kalaiselvam, *Mater. Res. Express*, **7**, 15045 (2020); https://doi.org/10.1088/2053-1591/ab6642
9. R. Trivedi, T.K. Upadhyay, M.H. Mujahid, F. Khan, P. Pandey, A.B. Sharangi, K. Muzammil, N. Nasir, A. Hassan, N.M. Alabdallah, S. Anwar, S. Siddiqui and M. Saeed, *Processes*, **10**, 338 (2022); https://doi.org/10.3390/pr10020338
10. P. Rauwel, *Global J. Nanomedicine*, **1**, (2017); https://doi.org/10.19080/GJN.2017.01.555562
11. M. Rawat, J. Singh and H. Kaur, *J. Nanomed. Res.*, **7**, (2018); https://doi.org/10.15406/jnmr.2018.07.00191
12. A. Shyam, S.S. Chandran, B. George and E. Sreelekha, *Inorg. Nano-Metal Chem.*, **51**, 1646 (2021); https://doi.org/10.1080/24701556.2020.1852254
13. J. Qu, X. Yuan, X. Wang and P. Shao, *Environ. Pollut.*, **159**, 1783 (2011); https://doi.org/10.1016/j.envpol.2011.04.016
14. M.W. Alam, H.S. Al Qahtani, M. Aamir, A. Abuzir, M.S. Khan, N. Zaidi, M. Albuhulayqah, S. Mushtaq, and A. Ramya, *Polymers*, **14**, 1827 (2022); https://doi.org/10.3390/polym14091827
15. R.R. Banala, V.B. Nagati and P.R. Karnati, *Saudi J. Biol. Sci.*, **22**, 637 (2015); https://doi.org/10.1016/j.sjbs.2015.01.007
16. R. Mukherjee, D. Talukdar, P. Mukherjee, S. Guha, G.K. Mandal, D. Mitra, R. Naskar, S. Mandal, N. Alam, S.K. Sahu, B. Majumder, G. Das and N. Murmu, *ChemistrySelect*, **10**, e202405116 (2025); https://doi.org/10.1002/slct.202405116
17. S.P. Singh, A. Mishra, R.K. Shyanti, R.P. Singh and A. Acharya, *Biol. Trace Elem. Res.*, **199**, 1316 (2021); https://doi.org/10.1007/s12011-020-02255-z
18. R. Sankar, P. Manikandan, V. Malarvizhi, T. Fathima, K.S. Shivashangari and V. Ravikumar, *Spectrochim. Acta A Mol. Biomol. Spectrosc.*, **121**, 746 (2014); https://doi.org/10.1016/j.saa.2013.12.020
19. S. Sunkari, B.R. Gangapuram, R. Dadigala, R. Bandi, M. Alle and V. Guttena, *J. Anal. Sci. Technol.*, **8**, 13 (2017); https://doi.org/10.1186/s40543-017-0121-1
20. G. Das, H.-S. Shin and J.K. Patra, *Int. J. Nanomedicine*, **15**, 9075 (2020); https://doi.org/10.2147/IJN.S277625
21. A.S. Rodrigues, J.G.S. Batista, M.A.V. Rodrigues, V.C. Thipe, L.A.R. Minarini, P.S. Lopes and A.B. Lugão, *Front. Microbiol.*, **15**, 1440065 (2024); https://doi.org/10.3389/fmicb.2024.1440065
22. A, Sati, T.N. Ranade, S.N. Mali, H.K.A. Yasin and A. Pratap, A*CS Omega*, **10**, 7549 (2025); https://doi.org/10.1021/acsomega.4c11045
23. S. Sumitha, S. Vasanthi, S. Shalini, S.V. Chinni, S.C.B. Gopinath, P. Anbu, M.B. Bahari, R. Harish, S. Kathiresan and V. Ravichandran, *Molecules*, **23**, 3311 (2018); https://doi.org/10.3390/molecules23123311
24. I.A. Holder and S.T. Boyce, *Burns*, **20**, 426 (1994); https://doi.org/10.1016/0305-4179(94)90035-3
25. S. Magaldi, S. Mata-Essayag, C. Hartung de Capriles, C. Perez, M.T. Colella, C. Olaizola and Y. Ontiveros, *Int. J. Infect. Dis.*, **8**, 39 (2004); https://doi.org/10.1016/j.ijid.2003.03.002
26. S. Ahmed, Saifullah, M. Ahmad, B.L. Swami and S. Ikram, *J. Radiat. Res. Appl. Sci.*, **9**, 1 (2016); https://doi.org/10.1016/j.jrras.2015.06.006
27. S. Chen, S. Thota, X. Wang and J. Zhao, *J. Mater. Chem. A*, **4**, 9038 (2016); https://doi.org/10.1039/C6TA02914K
28. M.A. Salem, E.A. Bakr and H.G. ElAttar, *Spectrochim. Acta A Mol. Biomol. Spectrosc.*, **188**, 155 (2018); https://doi.org/10.1016/j.saa.2017.07.002
29. M. Bekmezci, H. Öztürk, M. Akin, R. Bayat, F. Sen, R. Darabi and H. Karimi-Maleh, *Biosensors*, **13**, 531 (2023); https://doi.org/10.3390/bios13050531
30. A.T.N. Dao, D.M. Mott, K. Higashimine and S. Maenosono, *Sensors*, **13**, 7813 (2013); https://doi.org/10.3390/s130607813
31. F. Zheng, S.Y. Luk, T.L. Kwong, K.F. Yung, *RSC Adv.*, **6**, 44902 (2016); https://doi.org/10.1039/c6ra06398e
32. W.A. Zoubi, A.A. Mahmud, F. Hazmatulhaq, M.R. Thalji, S. Leoni, J.-H. Kang and Y.G. Ko, *SusMat*, **4**, e216 (2024); https://doi.org/10.1002/sus2.216
33. V.K. Sharma, R.A. Yngard and Y. Lin, *Adv. Colloid Interface Sci.*, **145**, 83 (2009); https://doi.org/10.1016/j.cis.2008.09.002
34. I.A. Holder and S.T. Boyce, *Burns*, **20**, 426 (1994); https://doi.org/10.1016/0305-4179(94)90035-3
35. B. Ranpariya, G. Salunke, S. Karmakar, K. Babiya, S. Sutar, N. Kadoo, P. Kumbhakar and S. Ghosh, *Front. Microbiol.*, **11**, 610968 (2020); https://doi.org/10.3389/fmicb.2020.610968
36. S. Magaldia, S. Mata-Essayaga, C.H. de Caprilesa, C. Pereza, M.T. Colella, C. Olaizola and Y. Ontiveros, *Int. J. Infect. Dis.*, **8**, 39 (2004); https://doi.org/10.1016/j.ijid.2003.03.002